remote sensing

MDPI

Article

A New and Robust Index for Water Body Extraction from Sentinel-2 Imagery

Zhenfeng Su [1], Longwei Xiang [1,*], Holger Steffen [2], Lulu Jia [3], Fan Deng [1], Wenliang Wang [1], Keyu Hu [1], Jingjing Guo [1], Aile Nong [1], Haifu Cui [1] and Peng Gao [4]

[1] School of Geosciences, Yangtze University, Wuhan 430100, China; suzhenfeng.st@yangtzeu.edu.cn (Z.S.); dengfan@yangtzeu.edu.cn (F.D.); wangwenliang.st@yangtzeu.edu.cn (W.W.); hukeyu.stu@yangtzeu.edu.cn (K.H.); guojingjing.stu@yangtzeu.edu.cn (J.G.); nongaile.stu@yangtzeu.edu.cn (A.N.); cuihaifu@yangtzeu.edu.cn (H.C.)
[2] Geodetic Infrastructure, Lantmäteriet, 80182 Gävle, Sweden; holger.steffen@lm.se
[3] Institute of Geophysics, China Earthquake Administration, Beijing 100081, China; jialulu@cea-igp.ac.cn
[4] School of Resources and Environment, Linyi University, Linyi 276000, China; gaopeng@lyu.edu.cn
* Correspondence: lwxiang@yangtzeu.edu.cn

Abstract: Land surface water is a key part in the global ecosystem balance and hydrological cycle. Remote sensing has become an effective tool for its spatio-temporal monitoring. However, remote sensing results exemplified in so-called water indices are subject to several limitations. This paper proposes a new and effective water index called the Sentinel Multi-Band Water Index (SMBWI) to extract water bodies in complex environments from Sentinel-2 satellite imagery. Individual tests explore the effectiveness of the SMBWI in eliminating interference of various special interfering cover features. The Iterative Self-Organizing Data Analysis Technique Algorithm (ISODATA) method and confusion matrix along with the derived accuracy evaluation indicators are used to provide a threshold reference when extracting water bodies and evaluate the accuracy of the water body extraction results, respectively. The SMBWI and eight other commonly used water indices are qualitatively and quantitatively compared through vision and accuracy evaluation indicators, respectively. Here, the SMBWI is proven to be the most effective at suppressing interference of buildings and their shadows, cultivated lands, vegetation, clouds and their shadows, alpine terrain with bare ground and glaciers when extracting water bodies. The overall accuracy in all tests was consistently greater than 96.5%. The SMBWI is proven to have a high ability to identify mixed pixels of water and non-water, with the lowest total error among nine water indices. Most notably, better results are obtained when extracting water bodies under interfering environments of cover features. Therefore, we propose that our novel and robust water index, the SMBWI, is ready to be used for mapping land surface water with high accuracy.

Keywords: Sentinel-2; water index; water body extraction; confusion matrix; ISODATA

check for updates

Citation: Su, Z.; Xiang, L.; Steffen, H.; Jia, L.; Deng, F.; Wang, W.; Hu, K.; Guo, J.; Nong, A.; Cui, H.; et al. A New and Robust Index for Water Body Extraction from Sentinel-2 Imagery. *Remote Sens.* **2024**, *16*, 2749. https://doi.org/10.3390/rs16152749

Academic Editor: Teodosio Lacava

Received: 30 November 2023
Revised: 18 July 2024
Accepted: 21 July 2024
Published: 27 July 2024

Copyright: © 2024 by the authors. Licensee MDPI, Basel, Switzerland. This article is an open access article distributed under the terms and conditions of the Creative Commons Attribution (CC BY) license (https://creativecommons.org/licenses/by/4.0/).

1. Introduction

As invaluable parts of the global ecosystem balance and hydrological cycle, land surface water (LSW) bodies, such as rivers, lakes and reservoirs, provide fundamental resources to terrestrial life and the climate system [1–3]. Their accurate spatio-temporal surveying is therefore a prerequisite for understanding hydrology processes, managing water resources as well as predicting and preventing floods [1,4–6]. However, traditional terrestrial hydrological field measurements often reach their limits given the partly scattered distribution of LSW bodies on the tremendous surface area of the Earth, where some are even located in challenging climatic conditions, rough terrain or areas with scarce infrastructure (such as in the Tibetan Plateau). Here, instead of traditional field measurements, mapping inundation areas using remote sensing has become the most efficient approach [2,6].

In the past four decades, remote sensing has been widely applied in LSW mapping, as this technology has the advantages of being macrographic, dynamic, real-time as well as low-cost, which is substantially different from conventional in situ measurements [1,2]. Satellite sensors of varying temporal and spatial resolutions, such as Landsat, Sentinel, Gaofen, Ziyuan, MODIS, SPOT and WorldView, have been used to extract water body information for hydrology or/and environmental change studies [2,7–14]. LSW changes derived from remote sensing can also be combined with GIS techniques for various applications including flood hazard/damage assessment and management [15,16].

Numerous remote sensing methodologies have been proposed to map surface water bodies. Huang et al. [7] and Rad et al. [17] grouped them into the three categories of density slicing with a threshold, machine learning and spectral water indices, and they summarized the characteristics of the methods: the density slicing methods are the simplest but very inaccurate in noise-abundant images [18]; machine learning methods require a large amount of data to train, thus being computationally demanding in training and retraining processes [19]; and spectral water indices are effective methods, which can be implemented and transferred across platforms easily with low computation costs, meaning they are widely used to understand lake water quality, water levels and other conditions in a timely manner with satellite image data, conducive to the implementation of water resource protection and management.

Based on their many advantages, various water indices were developed in recent years. McFeeters [20] introduced the Normalized Difference Water Index (NDWI), which uses the strong contrast between visible light and near-infrared light to highlight water information when extracting water bodies. Xu [21] proposed the Modified Normalized Difference Water Index (MNDWI), which effectively extracts water bodies within urban areas. Wu et al. [22] developed the Vegetation Red-Edge-based Water Index (RWI), which eliminates the influence of mountains, building shadows and clouds. Cao et al. [23] presented the Revised Normalized Difference Water Index (RNDWI) to accurately extract the water–land boundary, weakening the influence of terrain shadows. Wang et al. [24] promoted the Multi-Band Water Index (MBWI), which can weaken the influence of mountain shadows and buildings by combining information from multiple bands. Feyisa et al. [9] proposed the Automated Water Extraction Index shortwave ($AWEI_{sh}$) and Automated Water Extraction Index narrow shortwave ($AWEI_{nsh}$) using the shortwave infrared and near-infrared bands to extract water information from high-resolution imagery. Chen et al. [25] developed the Shadow Water Index (SWI) method, which can better differentiate water bodies and shadows and weaken the influence of snow and bare ground in mountainous areas.

The water indices mentioned above have promoted countless studies on extracting water body information from remote sensing images. However, as Li et al. [26] stated, the existing water indices still have their limitations, such as identifying small water bodies, distinguishing water bodies from glaciers, snow and/or clouds and extracting urban surface water bodies within a complex land cover structure [11,27].

Therefore, aiming to improve the efficiency of water body extraction, this paper proposes a new and robust water index based on Sentinel-2 satellite images, which is effective in complex environments. To verify the validity of our new water index, we select six sites for tests of its effectiveness in extracting water bodies under different specific interference(s), respectively.

In the next section, the six test sites and data sources are introduced. In Section 3, the process of the water index construction is shown, followed by the presentation and discussion of the testing results in Sections 4 and 5, respectively. Finally, we summarize our findings in Section 6.

2. Study Areas and Data Sources

2.1. Test Site Selection

To assess the effectiveness of the proposed new water index, we selected the following six test sites with distinct typical interference(s): (1) urban built-up area, (2) heavy vege-

tation and clouds, (3) eutrophication and urban built-up shadows, (4 + 5) alpine terrain with bare ground and glaciers, and (6) mixed-edge pixels. They are all located in China (see Figure 1) and will be described in more detail below.

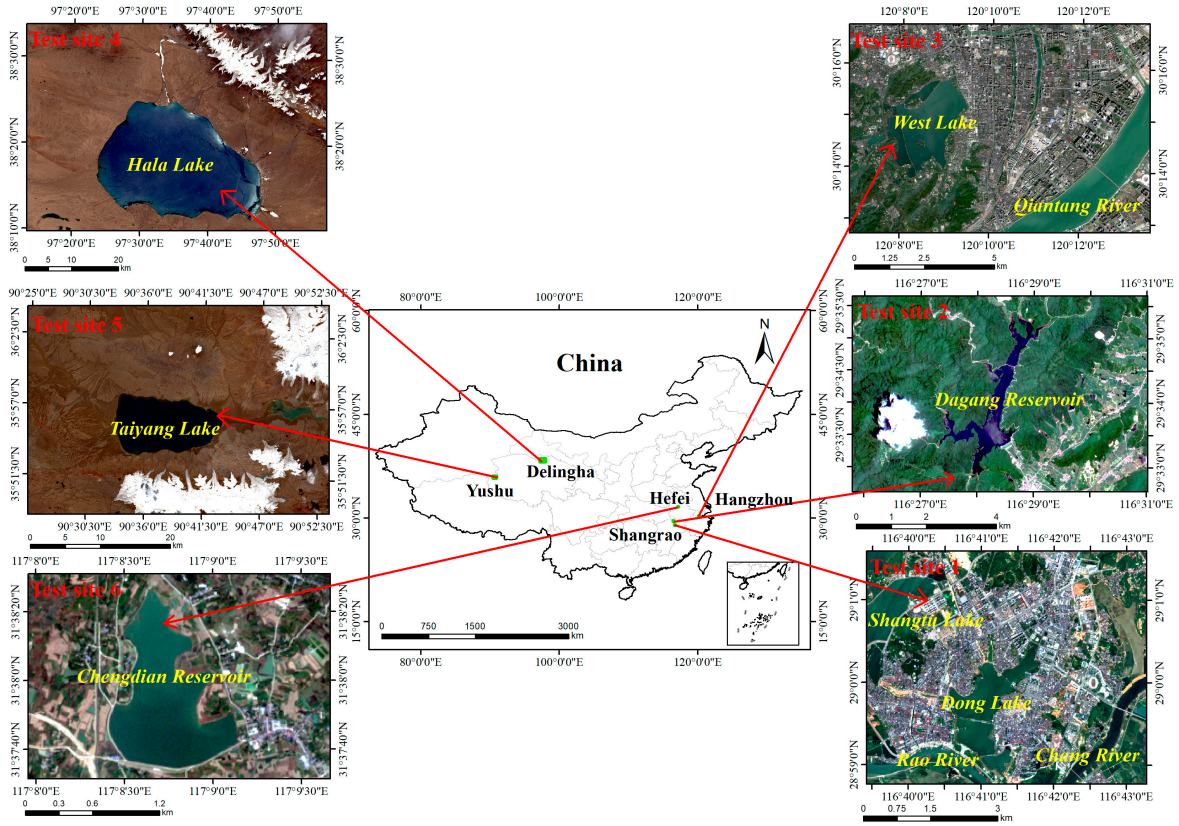


Figure 1. Locations of the six test sites. Test site 1: Dong Lake. Test site 2: Dagang Reservoir. Test site 3: West Lake. Test site 4: Hala Lake. Test site 5: Taiyang Lake. Test site 6: Chengdian Reservoir.

2.1.1. Urban Built-Up Area

To test the effectiveness of eliminating urban built-up interference, we selected Dong Lake in Poyang County (Shangrao city). The lake is surrounded by dense urban buildings (shown in Figure 1) and thus represents the perfect site for testing the effectiveness of the water index for removing urban buildings' disturbance. Besides its dense buildings, Dong Lake is also surrounded by other water bodies, namely the Rao River (Raohe), Chang River (Changjiang), Shangtu Lake (Shangtuhu) and several other pools or small lakes. This area is test site 1.

2.1.2. Vegetation and Clouds

The Dagang Reservoir is located in the north of Duchang County (Jiangxi Province) on the north shore of Poyang Lake and is the second largest reservoir in Jiujiang city. It is surrounded by hills covered with very dense vegetation (see Figure 1), making it very suitable for this test. At the same time, to consider the unavoidable existence of cloud interference in satellite images, this experiment retains a cloud and its shadows in the Sentinel-2 satellite images used. In addition, there are also many scattered small artificial reservoirs on the right side of Dagang Reservoir. Therefore, the Dagang Reservoir and its surroundings were selected as test site 2.

2.1.3. Eutrophication and Urban Built-Up Shadows

The increase in organic matter contents such as aquatic plants in a water body may lead to a reflectance like that of non-aquatic environments such as lakeshore vegetation,

potentially disrupting the accuracy of water body extraction [28]. To explore whether water indices are impacted by eutrophication in water bodies, we selected West Lake in the West Lake District of Hangzhou city (Zhejiang Province). This lake is affected by eutrophication, which is more severe along the shorelines compared with the lake center [29]. Moreover, numerous high-rise buildings surround it, and their casting shadows may affect the precision of water body extraction [30]. Adjacent to West Lake is the Qiantang River, which is also bordered by extensive high-rise buildings casting their shadows. We marked this area as test site 3.

2.1.4. Alpine Terrain with Bare Ground and Glaciers

Hala Lake is a closed alpine lake at 4078 m altitude located in the Qilian Mountains at the northeastern edge of the Tibetan Plateau. Its catchment is an endorheic basin with an area of 4793 km^2, which makes it a brackish lake, and the basin boundaries are alpine mountains with glaciers (and snow) on them. In addition, due to the harsh weather conditions and the challenging geography, there is only bare ground with barely any vegetation in the basin (Figure 1). It is a typical site for alpine bare ground and glaciers' interference testing. We marked it as test site 4. Taiyang Lake, our additional test site 5, has similar environments. It serves as additional testbed for our new approach. Corresponding results are presented in the Appendix A.

2.1.5. Mixed Pixels

Any lakeshore pixel containing both water and non-water surfaces is considered a mixed pixel (or mixed edge pixel). To investigate the sensitivity of different water indices in distinguishing between water and non-water in mixed pixels, we select the Chengdian Reservoir in Feixi County, Hefei city, Anhui Province. The lakeshore of Chengdian Reservoir is special, with winding curves and relatively gentle slopes. Such terrain conditions make it easier for individual pixels to concurrently contain multiple types of land cover, resulting in a higher occurrence of mixed water and non-water pixels. Additionally, the reservoir is surrounded by farmland and vegetation, providing an ideal testbed to investigate the sensitivity of different water indices in distinguishing mixed water and non-water pixels. Thus, here, we marked Chengdian Reservoir as test site 6.

2.2. Image Data

This study uses Sentinel-2 optical remote sensing images (Table 1). Sentinel-2 is a wide-swath, high-resolution, multi-spectral imaging satellite mission launched by the European Space Agency (ESA) and has been successfully applied in surface water mapping [1,2,31,32]. The images are available from the ESA website (https://scihub.copernicus.eu/dhus/#/home, accessed on 14 May 2023). Sentinel-2 image data have their advantages of high temporal and spatial resolution, rich band information and free data availability. We selected clear images without clouds (except test site 2 for the cloud interference test, see Table 1) for the specific interference removal testing.

Table 1. Sentinel-2 image information for the six test sites with an overview of the main land cover features.

Test Site	Location	Satellite	Acquisition Date	Typical Land Cover Features
1	Dong Lake (Shangrao)	Sentinel-2B	10 July 2022	Water bodies, urban buildings, vegetation, cultivated lands
2	Dagang Reservoir	Sentinel-2B	10 July 2022	Water bodies, dense vegetation, cloud and its shadow, cultivated lands
3	West Lake	Sentinel-2B	14 March 2023	Water bodies, urban buildings and its shadow, dense vegetation
4	Hala Lake	Sentinel-2A	23 May 2022	Water bodies, alpine terrain, glacier, bare ground
5 *	Taiyang Lake	Sentinel-2B	22 September 2022	Water bodies, alpine terrain, glacier, bare ground
6	Chengdian Reservoir	Sentinel-2B	7 November 2020	Water bodies, cultivated lands, vegetation, bare ground

* Results are presented and discussed in the Appendix A.

2.3. Image Preprocessing

We use the Sentinel-2 Level 2A S2MSI2A product type. This is an orthorectified and UTM geocoded product covering 110 × 110 km, providing Bottom-Of-Atmosphere reflectance and basic pixel classification. It is already subject to atmospheric correction, and thus only resampling and image fusion are necessary. We performed bicubic resampling using the Sentinels Application Platform (SNAP) (version 9.0.0) to resample the different-resolution original data into band data with a 10 m spatial resolution. Then, band fusion was performed using ENVI software (version 5.6) to obtain an image of the same spatial resolution for each testing site. Band parameters of the Sentinel-2 imagery used are presented in Table 2.

Table 2. Band parameters of Sentinel-2 data.

Bands	Central Wavelength (nm)	Resolution (m)
Band1-Coastal Aerosol	443	60
Band2-Blue	490	10
Band3-Green	560	10
Band4-Red	665	10
Band5-Vegetation Red Edge 1	705	20
Band6-Vegetation Red Edge 2	740	20
Band7-Vegetation Red Edge 3	783	20
Band8-Near Infrared	843	10
Band8A-Vegetation Red Edge 4	865	20
Band9-Water Vapor	945	60
Band10-Shortwave Infrared 1	1375	60
Band11-Shortwave Infrared 2	1610	20
Band12-Shortwave Infrared 3	2190	20

3. Methodology

3.1. Spectral Separability of Land Cover Features

To construct a new water index that effectively extracts water bodies in complex environments, it is necessary to calculate the average reflectance spectrum of various typical land cover features and find suitable bands for the index construction by referring to the characteristics of the reflectance curves [9].

In this study, reflectance spectra from Sentinel-2 remote sensing imagery were used to categorize typical ground objects into water bodies and non-water bodies. The non-water-body types included vegetation, bare ground, buildings, glaciers, clouds, buildings/cloud shadows and cultivated lands, as listed in Table 1. Reflectance data were gathered from Sentinel-2 satellite imagery for two sites in the Poyang Lake Basin (Dong Lake for test site 1, and Dagang Reservoir for test site 2) and one site of Hala Lake (test site 4). The image of the Poyang Lake Basin was obtained on 10 July 2022, while the image of Hala Lake was captured on 23 May 2022. Water bodies at different places under varying environmental conditions may capture the spectral variability for land features across different environments due to lighting conditions, varying water depths and/or the different material contents in water bodies, such as the suspended solids and organic and inorganic materials [33]. At all three sites, the Minimum Noise Fraction Transform (MNFT) was used to reduce noise, and the Pixel Purity Index (PPI) was employed to calculate pure pixels after appropriate iterations. To help accurately identify pure pixel categories of different land features, time-suitable Google Maps high-resolution satellite images were used as a reference to confirm the land cover types of pure pixels. In this way, 2570, 1460 and 740 pure pixels of land features were extracted from reflective bands for test sites of Dong Lake, Dagang Reservoir and Hala Lake, respectively. The average reflectance values of these pure pixels are shown in Figures 2–4. We then investigate the spectral separability of Region of Interest (ROI) pairs of the major land cover features selected at the three test sites, using the Jeffries–Matusita

pairwise separability measure in ENVI (version 5.6), and all pairs of land cover types were found to be separable, with spectral separability values ranging from 1.98 to 2.0.

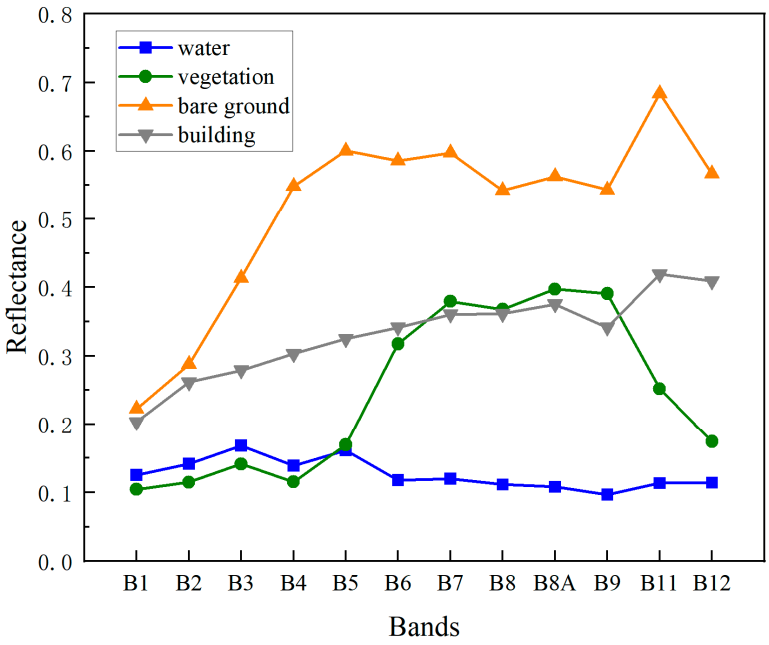


Figure 2. Spectral average reflectance(s) of typical land cover features at test site 1, Dong Lake. The horizontal axis are 12 bands of the multi-spectral data from Sentinel-2 satellite image, where B1 represents the coastal aerosol band, B2 blue, B3 green, B4 red, B5, B6, B7, B8 and B8A near-infrared and B9, B11 and B12 shortwave infrared, while the cirrus cloud estimation (B10) bands are not included here.

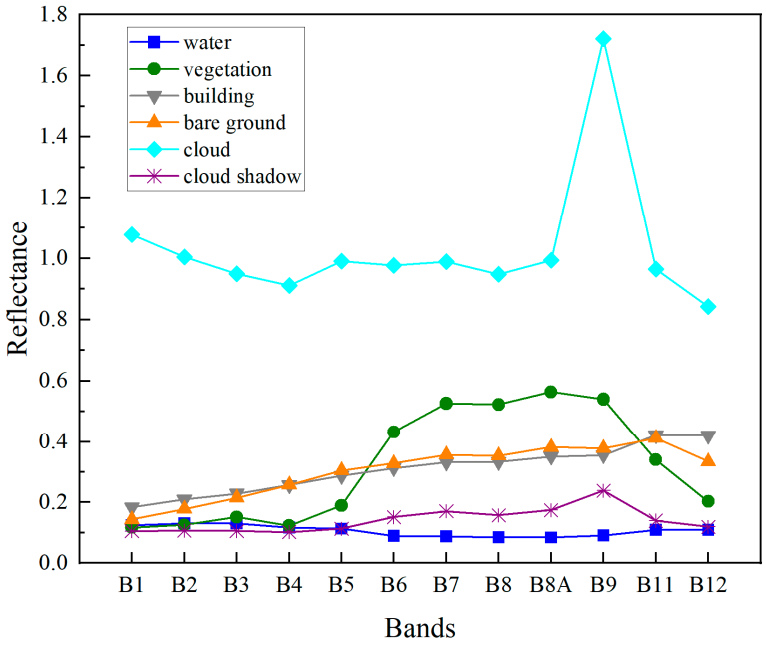


Figure 3. As Figure 2, but for spectral average reflectance(s) of typical land cover features at test site 2, Dagang Reservoir.

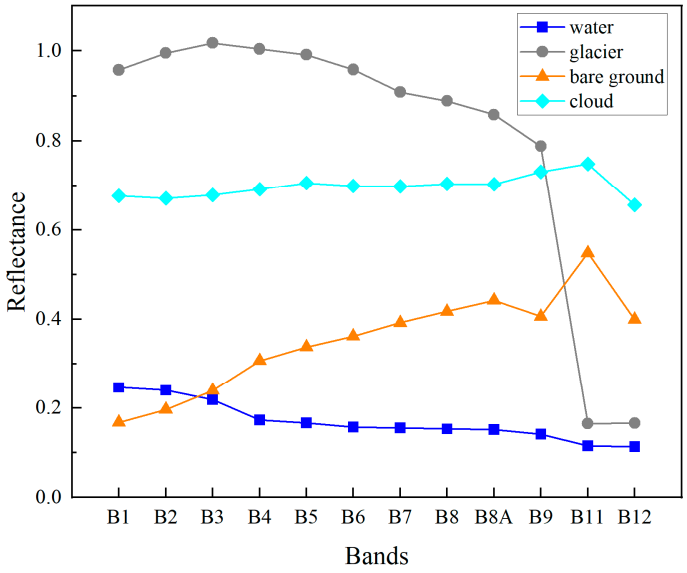


Figure 4. As Figure 2, but for spectral average reflectance(s) of typical land cover features at test site 4, Hala Lake.

3.2. Construction of the New Water Index

Constructing a new index should involve considering the reflectance spectrum characteristics of land cover features and follow the principle of enhancing the water signal and suppressing the background signal. Based on the average spectral reflectance curve characteristics of typical land cover features, and referring to the $AWEI_{sh}$ index [9], this study retained bands 2, 3, 8, 11 and 12. Further, through the curve characteristics, it was found that a water body has lower reflectance in near-infrared bands 8, 8A and 9, while non-water areas have higher reflectance. Therefore, the unique band 8A was included along with bands 8 and 9 as the subtrahend in the new water index. Meanwhile, we retained the additive terms $\rho_{band2} + 2.5\rho_{band3}$ of the $AWEI_{sh}$ index, which is stated to effectively suppress the effects of terrain-induced shadows and dark surfaces [9]. Finally, we propose a new water index called the Sentinel Multi-Band Water Index (SMBWI), which can be expressed in the following equation:

$$SMBWI = \rho_{band2} + 2.5\rho_{band3} - 2(\rho_{band8} + \rho_{band8A} + \rho_{band9}) - \rho_{band11} - \rho_{band12} \quad (1)$$

in which the weight coefficients were determined based on the effectiveness of the index after extensive testing. While ρ_{bandi} represents the reflectance of the *i*-th band of multi-spectral data from Sentinel-2 satellite image.

To investigate the accuracy and reliability of the new index, we compared the results of the SMBWI with eight commonly used water indices (see Table 3) at the six different test sites through vision and the assessment indicators stated in Section 4.

Table 3. Overview of the 8 commonly used water indices for comparison in this paper.

Water Index	Reference	Equation
NDWI	McFeeters [20]	$(\rho_{b3} - \rho_{b8})/(\rho_{b3} + \rho_{b8})$
RNDWI	Cao et al. [23]	$(\rho_{b12} - \rho_{b4})/(\rho_{b12} + \rho_{b4})$
MNDWI	Xu [21]	$(\rho_{b3} - \rho_{b11})/(\rho_{b3} + \rho_{b11})$
SWI	Chen et al. [25]	$\rho_{b2} + \rho_{b3} - \rho_{b8}$
RWI	Wu et al. [22]	$\frac{(\rho_{b3}+\rho_{b5}-\rho_{b8}-\rho_{b8A}-\rho_{b12})}{(\rho_{b3}+\rho_{b5}+\rho_{b8}+\rho_{b8A}+\rho_{b12})}$
MBWI	Wang et al. [24]	$2\rho_{b3} - \rho_{b4} - \rho_{b8} - \rho_{b11} - \rho_{b12}$
$AWEI_{sh}$	Feyisa et al. [9]	$\rho_{b2} + 2.5\rho_{b3} - 1.5(\rho_{b8} + \rho_{b11}) - 0.25\rho_{b12}$
$AWEI_{nsh}$	Feyisa et al. [9]	$4(\rho_{b3} - \rho_{b11}) - (0.25\rho_{b8} + 2.75\rho_{b12})$

Note that ρ_{bi} represents the reflectance of the *i*-th band of multi-spectral data from Sentinel-2 satellite image.

3.3. Analysis Methods

3.3.1. ISODATA Algorithm

The iterative Self-Organizing Data Analysis Technique Algorithm (ISODATA) calculates class means evenly distributed in the data space and then iteratively clusters the remaining pixels using minimum distance techniques [34]. ISODATA selects the initial class clustering center according to certain principles, and then calculates the standard deviation of each cluster and the distances between class centers. The smaller the distance, the larger the similarity and the more likely they belong to the same class. Iterative class splitting, merging and deleting are performed based on input threshold parameters, and this process continues until the average class spacing is less than the defined threshold [35].

All indices in this study use ISODATA to extract water bodies, which is an effective unsupervised classification method, avoiding manual selection of thresholds, making the classification results more objective and thus resulting in more robust results with higher accuracy than those from traditional thresholding methods with manual intervention [36].

3.3.2. Accuracy Assessment Method

We evaluated the accuracy of the water index extraction results using accuracy evaluation metrics based on the confusion matrix, including overall accuracy, kappa, producers' accuracy, users' accuracy, omission error and commission error [37]. For more accurate evaluation, we also used time-suitable Google Maps high-resolution satellite images to help identify non-water and water bodies.

Kappa Coefficient

Kappa coefficients are often used for consistency testing and are calculated based on the confusion matrix [38,39], which is an indicator for measuring classification accuracy. Kappa coefficients usually range from 0 to 1, and higher values indicate better classification. According to Liu et al. [37], the Kappa coefficient can be calculated using

$$Kappa = \frac{TP + TN - [(TP + FP)(TP + FN) + (FN + TN)(FP + TN)]}{TA^2 - [(TP + FP)(TP + FN) + (FN + TN)(FP + TN)]} \quad (2)$$

where TA denotes the total number of samples, TP denotes the number of correctly identified water pixels, TN is the number of correctly rejected non-water pixels, FP is the number of incorrectly identified water pixels and FN is the number of incorrectly identified non-water pixels.

Overall Accuracy

Overall Accuracy (OA) is a statistical measure with probability, which represents the proportion of accurately classified samples to all samples and is usually expressed in percent. A higher value indicates better classification. OA values can be calculated using [37,40]

$$OA = \frac{TP + TN}{TA}. \quad (3)$$

Producers' Accuracy and Omission Error

Producers' accuracy (PA) represents the probability that the ground truth reference data of a specific class are correctly classified. PA can be calculated using [40]

$$PA = \frac{TP}{TP + FN}, \quad (4)$$

which is also usually expressed in percent. The Omission Error (OE) is a complement of the PA, referring to the probability of a specific class being missed or overlooked during the classification process, with the relationship $OE = 100\% - PA$.

Users' Accuracy and Commission Error

Users' accuracy (*UA*) refers to the conditional probability that a randomly selected sample from the classification map belongs to a class with the same ground-truth class. It reflects the reliability and confidence of each class in the classification map and is an important indicator for evaluating the classification results. *UA* is calculated using [40]

$$UA = \frac{TP}{TP + FP}. \quad (5)$$

The Commission Error (*CE*) is a complement of the *UA*, referring to the probability of a specific class being incorrectly classified, with the relationship $CE = 100\% - UA$.

3.3.3. Sub-Pixel Accuracy Assessment

The sub-pixel accuracy assessment evaluates the sensitivity of different water indices to mixtures of water and non-water bodies. In these mixed pixels, those with a water content exceeding 50% should theoretically be classified as water pixels, while those with a water content less than 50% should be classified as non-water pixels (see Figure 5).

The experiment was based on high-spatial-resolution Google Earth imagery of a close date to the target image, with manually interpreted boundaries serving as the true boundaries. In the sub-pixel accuracy assessment, it is assumed that the error impact of manually interpreted true water boundaries is negligible [9]. The true water boundary line divides a pixel into two parts when it passes through the raster. The area within the closed boundary line is considered water, and the other part is considered non-water. Then, according to the proportion of the water area in the pixel, six statistical intervals are set up: 0–10%, 10–30%, 30–50%, 50–70%, 70–90% and 90–100%, representing the interval range of the water content proportion in mixed pixels. In each interval, 10 pixels are randomly selected, totaling 60 pixels, to build a spectral library of mixed pixels with different water content proportions. To accurately identify mixed pixels with varying water content proportions, the Spectral Angle Mapper method of the ENVI software (version 5.6) was used to detect these pixels. Subsequently, a true water body boundary mask was applied to the detected pixels to ensure that the boundaries of the mixed pixels accurately reflect their actual distribution on the ground surface. This process allows for the precise differentiation and quantification of the varying water content proportions within these mixed pixels.

In the sub-pixel accuracy assessment of various water indices, the true water boundaries are superposed with the extracted boundaries, using the water index to assess the accuracy of the index in detecting mixed pixels. Using Python's GDAL library (version 3.4.3) and NumPy (version 1.22.4), differential calculations and statistical analysis are performed to quantify the commission and omission errors caused by the lakeshore mixed pixels. Specifically, in the mixed pixels identified by the index, any portion that extends beyond the true boundary is considered a sub-pixel-level commission error. Conversely, parts of mixed non-water pixels that fall inside the true water body are identified as omission errors [9].

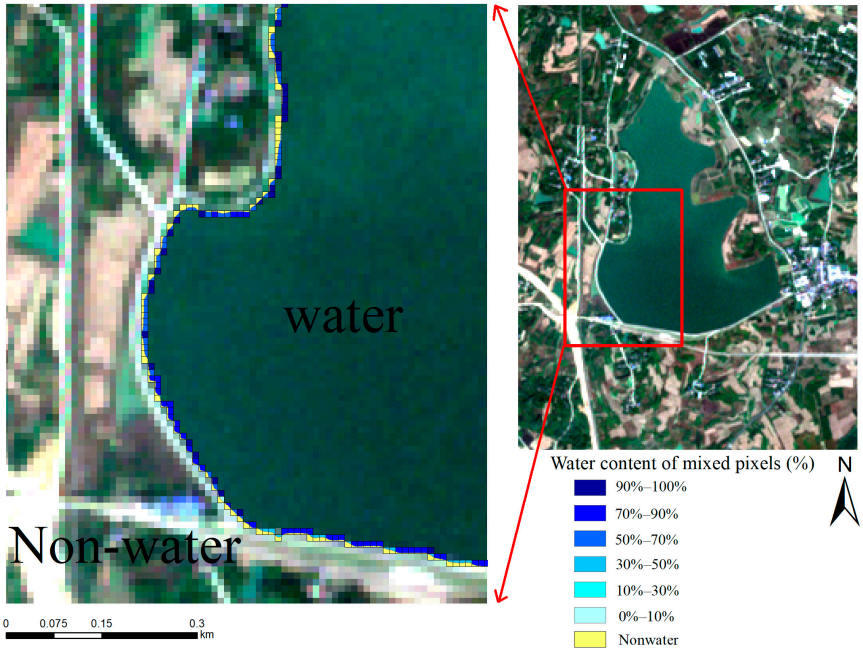


Figure 5. Mixed Pixel Classification at the lakeshore of Chengdian Reservoir. The right side of the image presents a general view of Chengdian Reservoir, while the left side is a magnified section showing the distribution and water content in mixed pixels.

4. Results

4.1. Urban Built-Ups' Interference-Eliminating Test

The water body extraction results derived from the SMBWI and the other eight water indices are shown for test site 1, Dong Lake, in Figure 6b–j, where non-water areas are in black, while water bodies are in white, with tiny white patches of mis-extraction by water indices, where the concentrated patches are delimited by red lines. Figure 6 shows that all the indices extracted water bodies, but those extracted by the SMBWI are more accurate, especially avoiding mis-extraction of various cover features as water bodies. When comparing the extraction results, the SMBWI, RWI, $AWEI_{nsh}$ and MBWI have fewer white patches outside the water bodies, with mis-extraction mainly concentrated on the southwest and on the northeast of Dong Lake, as delimited by red lines. In these two areas, the SMBWI has the fewest mis-extractions, followed by the RWI, $AWEI_{nsh}$ and MBWI. There are more mistakenly extracted cover features in other extraction results, whereas the SWI performs the worst. We randomly selected a local area on the original image and enlarged it, which is shown in Figure 7. The blue dots represent areas identified as water by the water indices. The SMBWI shows nearly no mis-extraction on building surfaces, whereas the RNDWI shows many more blue patches, and the SWI almost mistakenly extracted all urban built-up areas as water bodies. Regarding the mistakenly extracted cultivated lands southwest of Dong Lake, the SMBWI exhibited fewer mis-extractions, correctly and more effectively distinguishing farmlands from water bodies. In contrast, the RNDWI and SWI frequently misidentified these areas as water bodies, as shown in Figure 8.

Based on high-resolution satellite imagery provided by Google Maps, 140 water body validation sample points and 310 non-water-body validation sample points were selected. We evaluated our results quantitatively using seven indicators, as shown in Table 4. The Kappa and OA values of the nine water indices were generally consistent with our qualitative analysis; the SMBWI had the highest OA values and Kappa of 98.00% and 0.95, respectively, followed by the RWI, MBWI and $AWEI_{nsh}$ with high Kappa and OA values. Concerning the PA, UA, OE and CE indicators, the SMBWI also performed the best with the lowest total error (TE) of 6.48%.

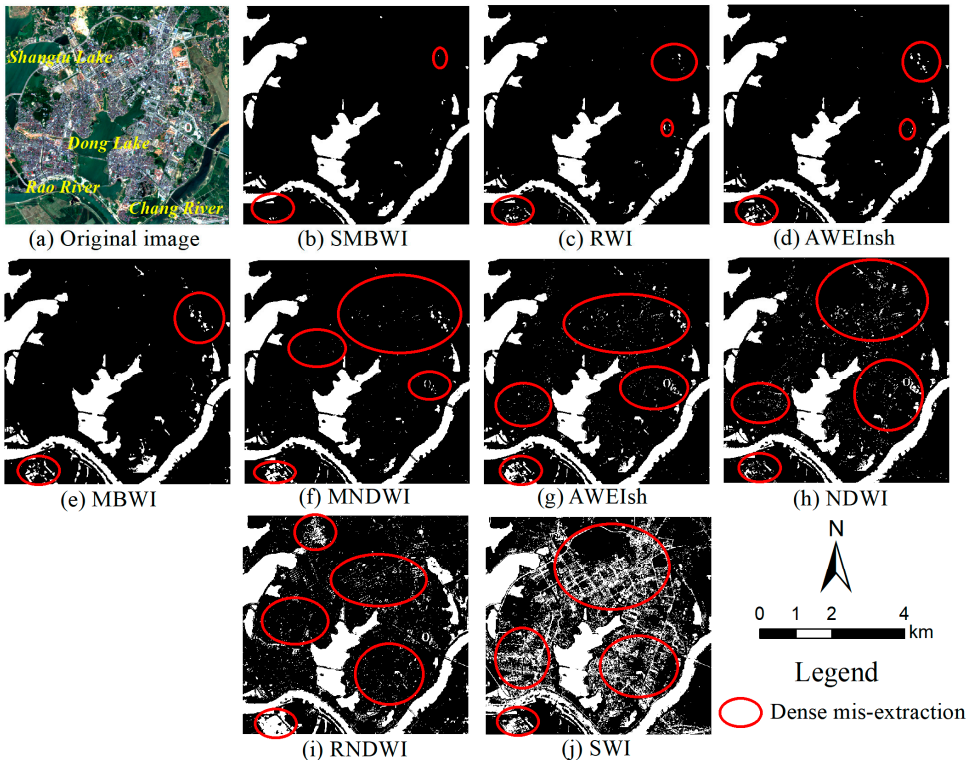


Figure 6. Water extraction results of the urban built-up area interference-eliminating test at test site 1, Dong Lake. (**a**) Original image of the test site; (**b**–**j**) extraction results from the corresponding water index. Note that the extracted water bodies are in white, while apart from real water bodies, a fairly substantial portion of the tiny white patches comprises mis-extraction of various other cover features by water indices. Red lines delimit the concentrated mis-extraction patches.

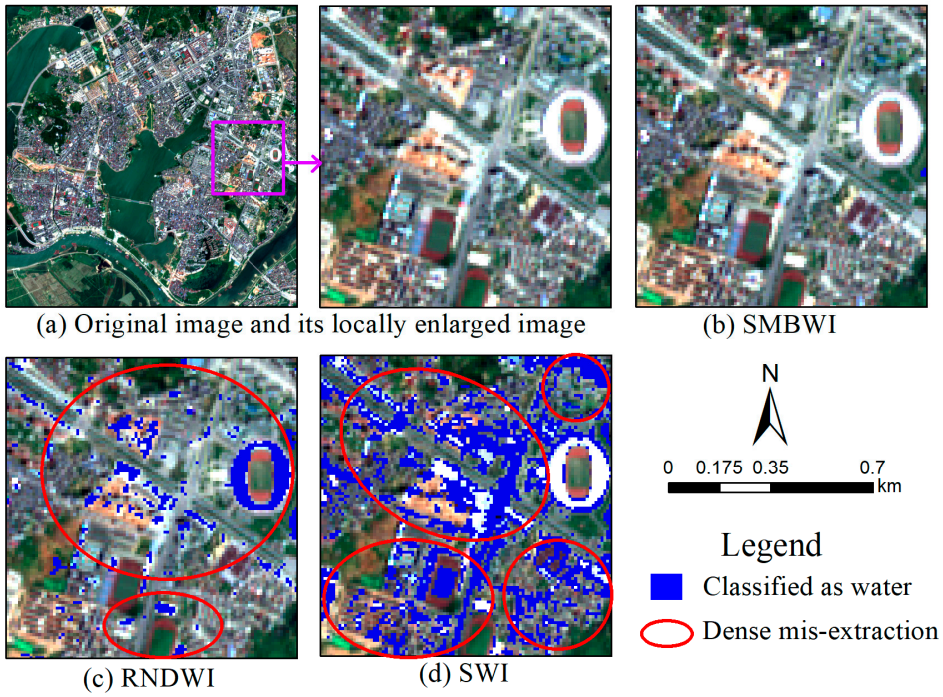


Figure 7. Local area extraction results of the urban built-ups' interference-eliminating test for the best-performing and worst-performing indices. (**a**) Original image and its local enlarged image. (**b**–**d**) Water body extraction results in blue by SMBWI, RNDWI and SWI, respectively, overlying the original image. Red lines delimit the mis-extractions.

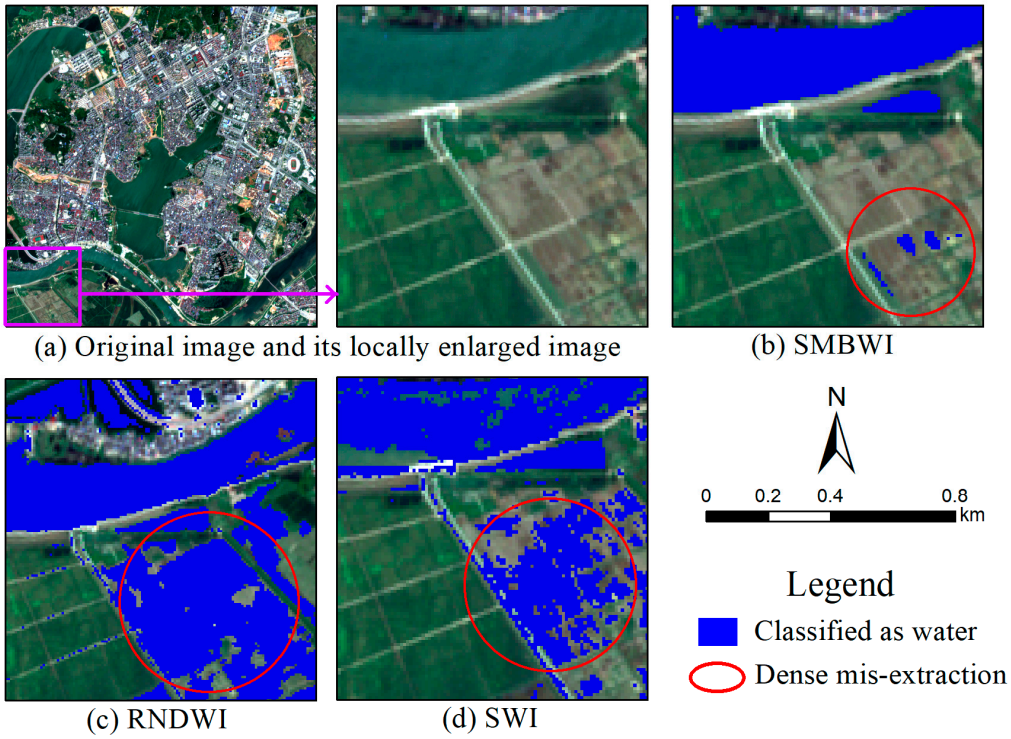


Figure 8. As Figure 7, but for cultivated lands' interference-eliminating test corresponding to Figure 6b,i,j.

Table 4. Accuracy assessment of the urban built-up interference-eliminating test.

Test Site	Water Index	OA (%)	Kappa	PA (%)	UA (%)	OE (%)	CE (%)	TE (%)
1 (Dong Lake)	SMBWI	98.00	0.95	95.71	97.81	4.29	2.19	6.48
	RWI	95.33	0.89	95.48	97.69	4.52	2.31	6.83
	MBWI	94.67	0.88	99.29	85.80	0.71	14.20	14.91
	$AWEI_{nsh}$	93.78	0.86	95.71	85.90	4.29	14.10	18.39
	MNDWI	90.67	0.79	95.71	78.82	4.29	21.18	25.47
	$AWEI_{sh}$	89.11	0.77	98.57	74.59	1.43	25.41	26.84
	NDWI	86.67	0.72	96.43	71.05	3.57	28.95	32.52
	RNDWI	79.33	0.59	97.86	60.35	2.14	39.65	41.79
	SWI	76.22	0.52	92.14	57.33	7.86	42.67	50.53

Note that the abbreviations of seven indicators are Kappa for Kappa coefficients, OA for overall accuracy, PA for producers' accuracy, UA for users' accuracy, OE for omission errors, CE for commission errors and the Total Error (TE) as the sum of OE and CE [41].

4.2. Vegetation and Cloud Interference-Eliminating Test

The experiment using the Dagang Reservoir, test site 2, examined the effectiveness of water indices in eliminating the interference of vegetation and clouds when extracting water bodies. The extraction results are shown in Figure 9b–j. All nine indices performed well in distinguishing water bodies from vegetation: there is a complete and clear outline of the reservoir, and on its right, the artificial reservoirs are identified. However, some of the indices did not effectively shield from interference caused by farmland and villages when extracting water bodies, such as the SWI, MNDWI and RNDWI. They mistakenly identified the farmland and villages east or southeast of Dagang Reservoir as water bodies, as outlined by the red lines in Figure 9h–j. The SMBWI performed very well, accurately extracting the small water bodies of the many artificial reservoirs scattered on the right side of the Dagang Reservoir. We further assessed the identification of small water bodies by

water indices through the method of area error and found that the SMBWI had superior properties in extracting small water bodies. This is detailed in Appendix A.1.

Regarding cloud interference, most of the water indices cannot effectively eliminate such interference. However, the SMBWI was again found to be the most effective one, which almost completely eliminated cloud interference, except for a small number of white patches caused by cloud shadows (see Figure 10b). In contrast, the MNDWI and RNDWI were largely unable to eliminate the interference of clouds and cloud shadows (Figure 10c,d).

Based on high-resolution satellite imagery provided by Google Maps, 120 water body validation sample points and 320 non-water-body validation sample points were selected. According to the indicators (Table 5), the SMBWI is the best index with the highest OA and Kappa values of 97.50% and 0.94, respectively, and lowest TE of 9.25%, followed by the MBWI and NDWI. The worst indices, with the lowest Kappa and OA values, are the MNDWI and RNDWI.

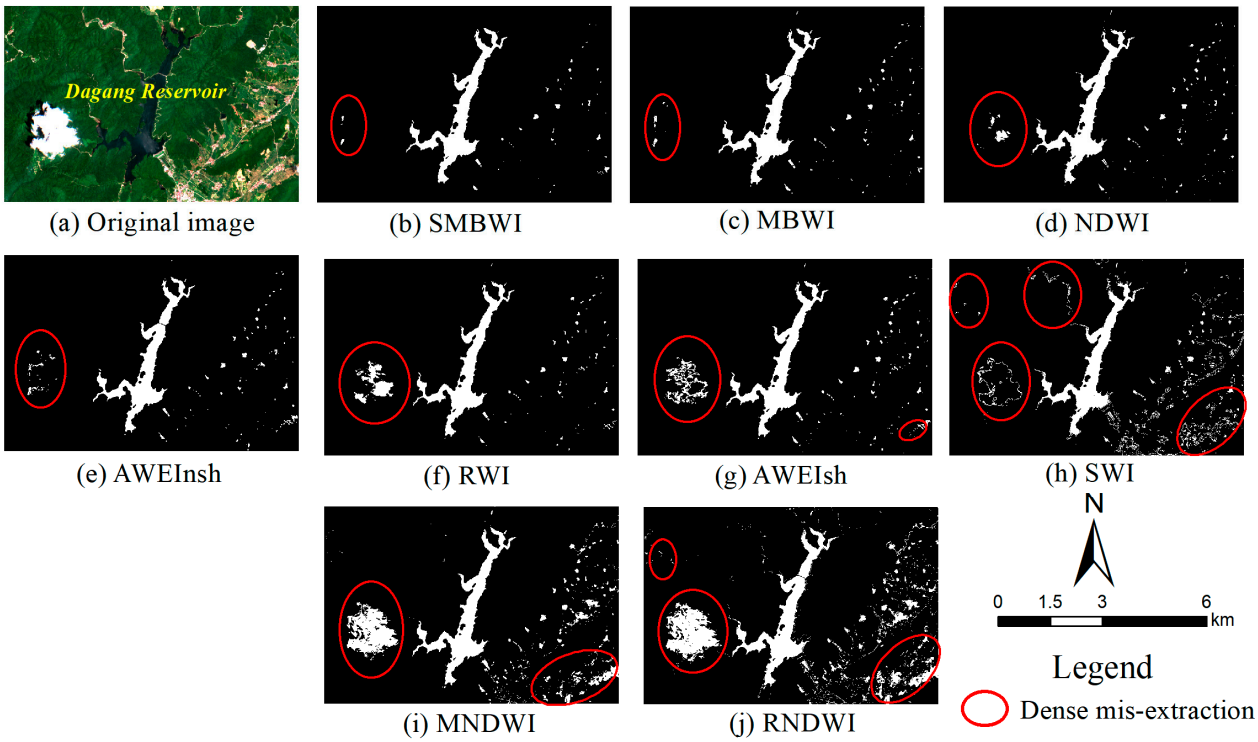


Figure 9. As Figure 6, but for the vegetation and cloud interference-eliminating test at test site 2, Dagang Reservoir.

Table 5. As Table 4, but for the vegetation and cloud interference-eliminating test.

Test Site	Water Index	OA (%)	Kappa	PA (%)	UA (%)	OE (%)	CE (%)	TE (%)
2 (Dagang Reservoir)	SMBWI	97.50	0.94	94.17	96.58	5.83	3.42	9.25
	MBWI	96.82	0.92	95.83	92.74	4.17	7.26	11.43
	NDWI	95.91	0.90	95.83	89.84	4.17	10.16	14.33
	$AWEI_{nsh}$	94.77	0.87	94.17	87.60	5.83	12.40	18.23
	RWI	93.64	0.85	95.00	83.82	5.00	16.18	21.18
	$AWEI_{sh}$	92.95	0.83	95.83	81.56	4.17	18.44	22.61
	SWI	91.14	0.79	93.33	78.32	6.67	21.68	28.35
	MNDWI	78.86	0.56	96.67	56.59	3.33	43.41	46.74
	RNDWI	76.36	0.52	95.83	53.74	4.17	46.26	50.43

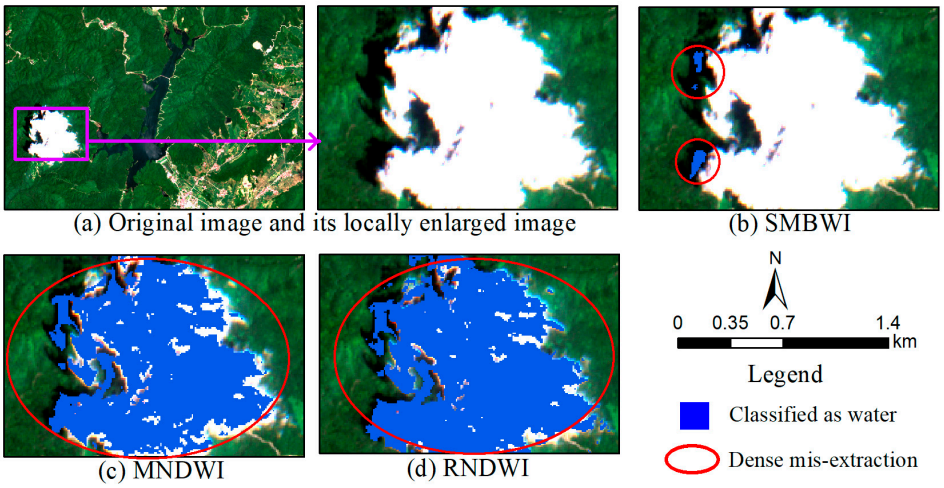


Figure 10. As Figure 7, but for the cloud and its shadows' interference-eliminating test corresponding to Figure 9b,i,j.

4.3. Eutrophication and Urban Built-Up Shadow Interference-Eliminating Test

To investigate whether aquatic plants affect the effectiveness of water indices in extracting water bodies, this study selected West Lake in Zhejiang Province as the experimental site. The extraction results shown in Figure 11b–j indicate that most water indices successfully extracted the water bodies of West Lake and the Qiantang River, and the SMBWI showed the best performance. To clearly demonstrate the extent to which water indices are affected by water eutrophication, Beili Lake, a sub-lake of West Lake, was selected for magnified display (see Figure 12a). The yellow lines highlight the densely eutrophic areas in this region. As shown in Figure 12b–j, most water indices are not affected by the eutrophic water bodies, the RNDWI is slightly affected, while the SWI is significantly impacted. In addition, some indices misidentified building shadows as water bodies to varying extents. Figure 13 clearly shows the mis-extraction of built-up areas' shadows by some indices. Meanwhile, the SMBWI shows minimal mis-extraction of building shadows, the RNDWI shows substantial mis-extraction of buildings and their shadows and the SWI fails in eliminating interference from buildings and their shadows.

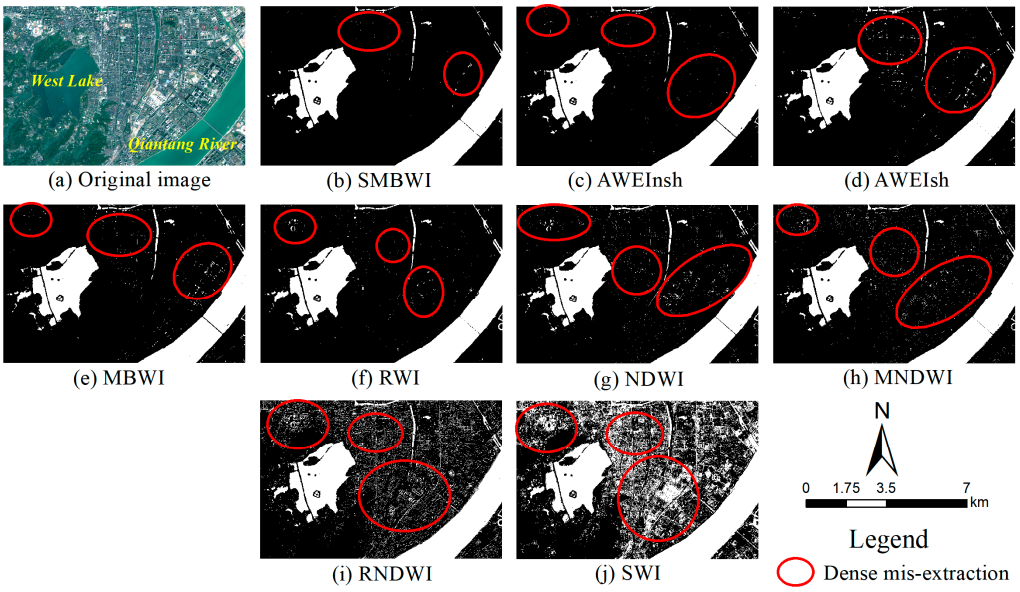


Figure 11. As Figure 6, but for the eutrophication and urban built-up shadow test at test site 3, West Lake.

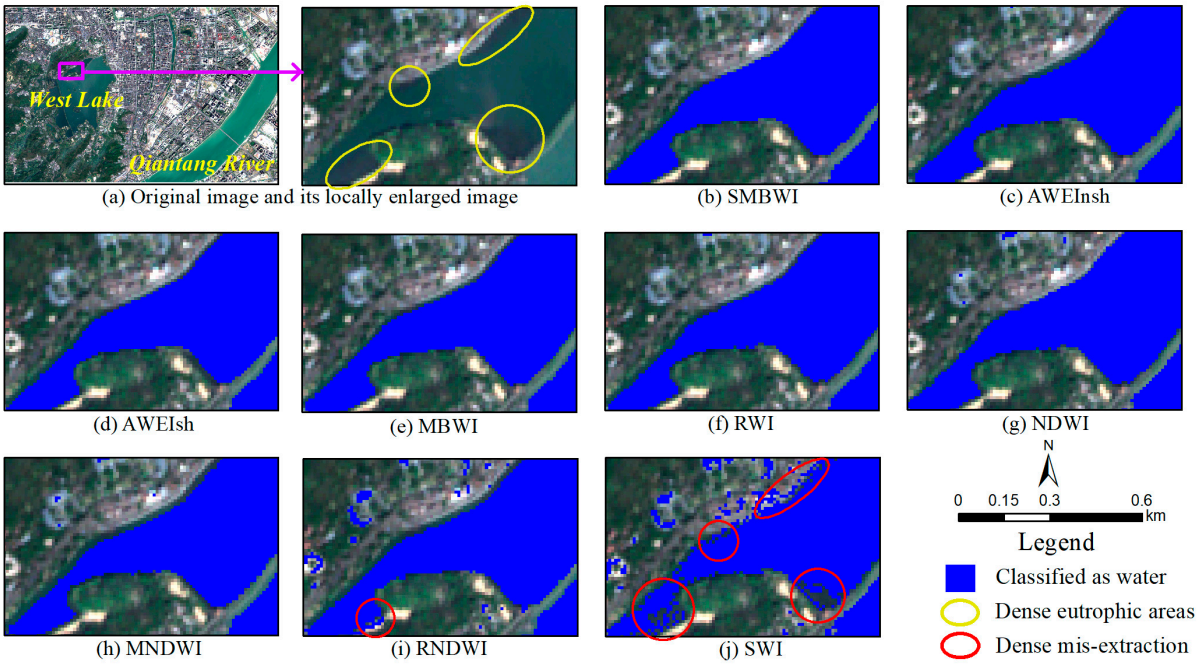


Figure 12. As Figure 11, but for the magnified display of Beili Lake.

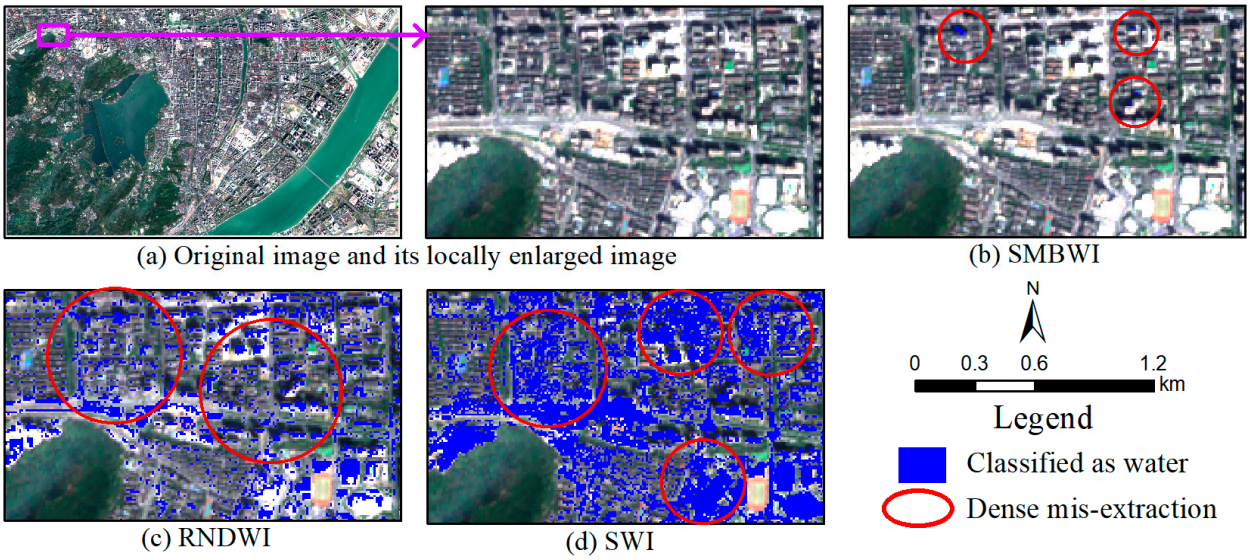


Figure 13. As Figure 7, but for urban built-up shadow interference-eliminating test corresponding to Figure 11b,i,j.

Based on high-resolution satellite imagery provided by Google Maps, 55 water body validation sample points and 150 non-water-body validation sample points were selected. The results of the seven indicators obtained from confusion matrix analysis and the Kappa values (see Table 6) show that the SMBWI performed best. The Kappa value reached 0.91, and the SMBWI had the highest overall accuracy (OA) of 96.59% and the lowest total error (TE).

Table 6. As Table 4 but for the eutrophication and urban built-up shadow interference test.

Test Site	Water Index	OA (%)	Kappa	PA (%)	UA (%)	OE (%)	CE (%)	TE (%)
3 (West Lake)	SMBWI	96.59	0.91	94.55	92.86	5.45	7.14	12.59
	$AWEI_{nsh}$	95.12	0.88	92.73	89.47	7.27	10.53	17.80
	$AWEI_{sh}$	93.17	0.83	94.55	82.54	5.45	17.46	22.91
	MBWI	92.20	0.81	92.73	80.95	7.27	19.05	26.32
	RWI	90.73	0.78	94.55	76.47	5.45	23.53	28.98
	NDWI	90.24	0.77	96.36	74.65	3.64	25.35	28.99
	MNDWI	89.27	0.75	92.73	73.91	7.27	26.09	33.36
	RNDWI	81.46	0.60	94.55	59.77	5.45	40.23	45.68
	SWI	70.73	0.44	96.36	47.75	3.64	52.25	55.89

4.4. Alpine Terrain and Glacier Interference-Eliminating Test

Due to having a similar spectral reflectance to water bodies, the presence of glaciers will affect water indices' extraction results. The Hala Lake Basin (test site 4, Figure 14a) in Qinghai Province was selected for testing of the potential for eliminating interference from alpine terrain with bare ground and glaciers. When comparing the extraction results in Figure 14b–j, it can be found that the nine indices performed well in distinguishing water bodies from alpine terrain with bare ground when extracting water bodies due to the significant difference in their reflectivity compared to that of water. However, the results extracted by the SMBWI provide the clearest and most precise appearance of Hala Lake as well as the small pools on its southwest. Apart from some white patches to the north of Hala Lake due to cloud shadow interference, the SMBWI performs extremely well. In Figure 15, referring to the original imagery with glaciers, extraction results from the three best- and worst-performing water indices are amplified to show the details. In these images, the blue areas represent water bodies extracted by the water indices. Specifically, the SMBWI shows no blue patches in glacier areas, demonstrating its strong ability to exclude non-water features, especially glaciers. In contrast, the RWI and RNDWI incur large blue areas where there are glaciers and clouds, indicating the indices' negative effects in these regions. To verify the reliability of the experiment, we conducted another investigation for Taiyang Lake, test site 5, which has a similar terrain to Hala Lake. The results are summarized in Appendix A.2 and confirm the excellent performance of the SMBWI.

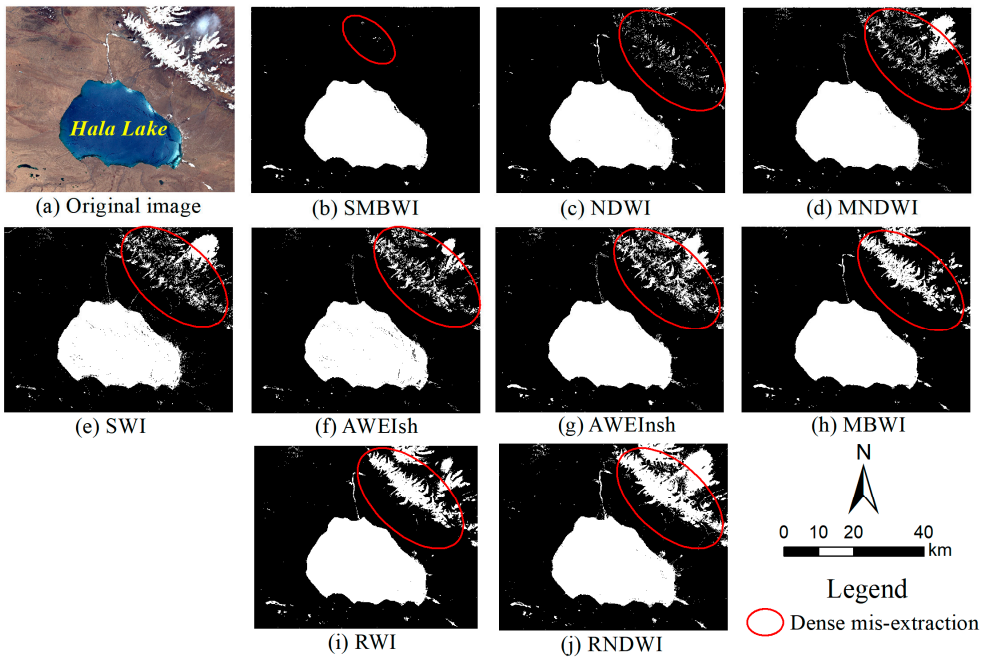


Figure 14. As Figure 6, but for the eliminating test of alpine terrain with bare ground and glaciers at test site 4, Hala Lake Basin.

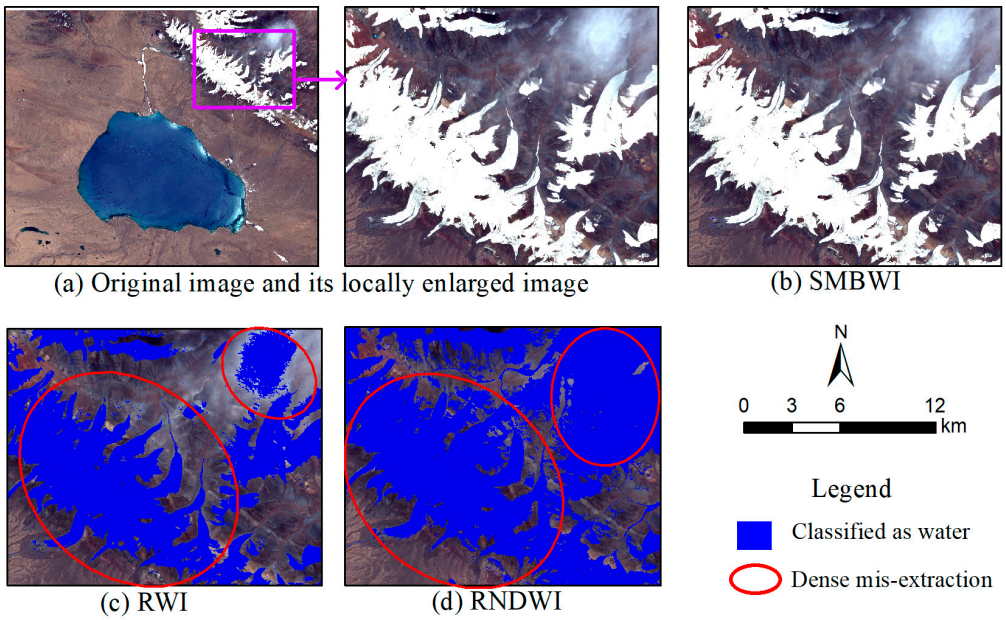


Figure 15. As Figure 7, but for glacier interference-eliminating test corresponding to Figure 14b,i,j.

Based on high-resolution satellite imagery provided by Google Maps, 300 water body validation sample points and 800 non-water-body validation sample points were selected. Again, the SMBWI showed the best results when using the evaluation indicators in Table 7.

Table 7. As Table 4, but for the eliminating test of alpine terrain with bare ground and glaciers.

Test Site	Water Index	OA (%)	Kappa	PA (%)	UA (%)	OE (%)	CE (%)	TE (%)
4 (Hala Lake)	SMBWI	99.64	0.99	99.00	99.66	1.00	0.34	1.34
	NDWI	93.37	0.84	97.67	81.62	2.33	18.38	20.71
	MNDWI	87.09	0.71	97.67	68.46	2.33	31.54	33.87
	SWI	84.45	0.65	95.33	64.56	4.67	35.44	40.11
	$AWEI_{sh}$	82.55	0.62	95.67	61.59	4.33	38.41	42.74
	$AWEI_{nsh}$	81.64	0.62	99.67	59.80	0.33	40.20	40.53
	MBWI	68.09	0.41	99.00	46.05	1.00	53.95	54.95
	RWI	63.00	0.34	98.00	42.30	2.00	57.70	59.70
	RNDWI	59.36	0.30	98.00	40.00	2.00	60.00	62.00

4.5. Mixed Pixel Test

This study explored the ability of nine different water indices to identify mixed pixels containing water and non-water bodies through sub-pixel-accuracy assessment at test site 6, Chengdian Reservoir (see Figure 5), located in the lower reaches of the Yangtze River Basin. At the test site, in total, there were 9754 mixed pixels and pure water pixels, of which 536 were mixed pixels, accounting for 5.50% of the total pixels. The number of pure water body pixels was 9218, representing 94.50% of the total pixels. Among the mixed pixels, those with a water content over 50% numbered 275, accounting for 51.31% of the total mixed pixels.

The precision assessment results for identifying mixed pixels with the nine water indices (see Table 8) showed that the SMBWI had the lowest total error of 18.84%, including an omission error of 10.63% and a commission error of 8.21%. This was followed by the $AWEI_{sh}$ index, with a total error of 23.32%, in contrast to the worst-performing index, the RNDWI, with the highest total error at 68.47%. Furthermore, an analysis of the mixed pixels' misclassification across different water content intervals (see Figure 16) revealed that, except for mixed pixels with a water content of 50–70%, the SMBWI had the lowest

classification error by total error (TE) in the other five water content proportion intervals among the nine water indices. Based on the statistical data of omission and commission errors and the total errors for the lakeshore mixed pixels, the SMBWI performed the best in identifying the mixed pixels among the nine water indices.

Table 8. The precision assessment results for identifying mixed pixels at test site 6, Chengdian Reservoir, with the nine water indices.

Test Site	Water Index	OE (%)	CE (%)	TE (%)
6 (Chengdian Reservoir)	SMBWI	10.63%	8.21%	18.84%
	$AWEI_{sh}$	8.21%	15.11%	23.32%
	RWI	12.50%	12.13%	24.63%
	MBWI	22.01%	3.73%	25.74%
	$AWEI_{nsh}$	19.78%	13.62%	33.40%
	NDWI	15.86%	18.10%	33.96%
	SWI	12.50%	23.13%	35.63%
	MNDWI	30.41%	20.52%	50.93%
	RNDWI	26.68%	41.79%	68.47%

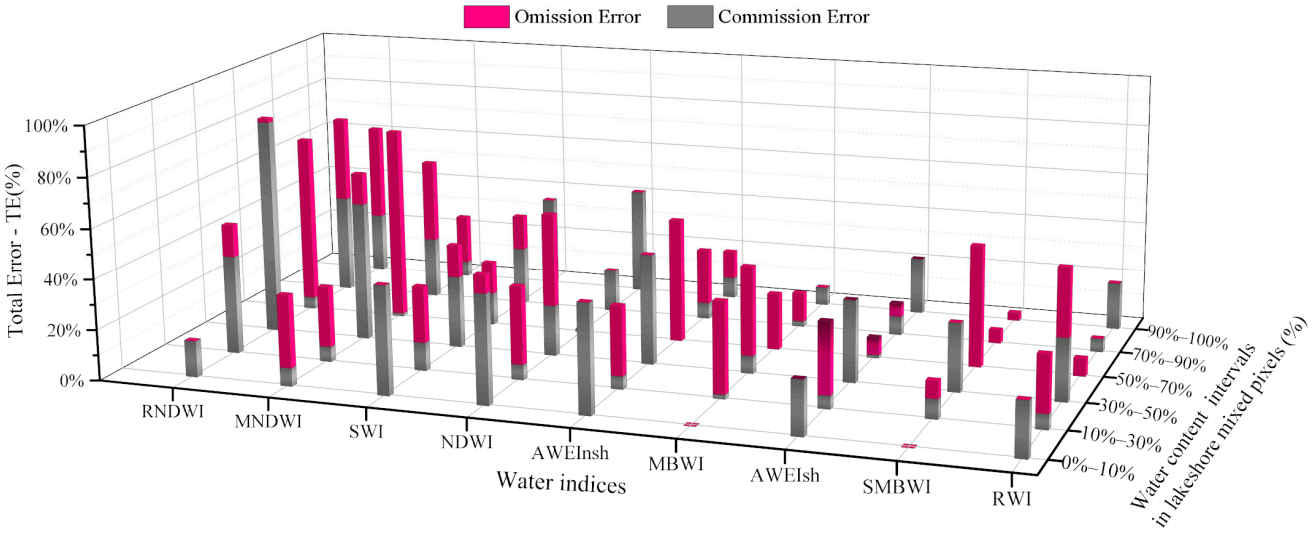


Figure 16. Statistical chart of omission errors and commission errors of all nine indices across six water content intervals for the lakeshore mixed pixel test at test site 6, Chengdian Reservoir.

5. Discussion

5.1. Mis-Extraction of Building Interference

When extracting water bodies from images with urban built-up areas using water indices, one important influencing factor is the diverse colors and materials of building surfaces that generate complex spectral reflectance, which might resemble the spectral characteristics of water [42,43]. This phenomenon often occurs on white rooftops, as shown in Figure 7c,d and Figure 13c,d.

Analyzing the formulas of the RNDWI and SWI reveals their difficulty in distinguishing between water bodies and buildings. The SWI uses only bands B2 (blue), B3 (green) and B8 (near-infrared) for water detection. However, as shown in Figures 2 and 3, the difference in reflectance between water bodies and buildings in the near-infrared and short-wave infrared bands is crucial for identification, and just depending on the B8 band (as in the SWI) is clearly insufficient for distinguishing water bodies from buildings effectively. Although the RNDWI includes band B12 (short-wave infrared), the reflectance values of water bodies in bands B4 (red) and B12 are relatively close. This may result in a normalized index value

close to zero since the key in the corresponding equation is to differentiate between the two, thereby affecting the effective distinction between water and non-water bodies.

Therefore, in constructing the SMBWI, we chose band B12 and did not use band B4, to optimize the classification performance. For the six test sites in this study, the performances of the RNDWI and SWI were often poor in terms of the Kappa coefficient and overall accuracy (OA), further confirming their inadequate classification effectiveness. In contrast, the SMBWI performed very well in combining multiple near-infrared and short-wave infrared bands, significantly enhancing the distinction between water bodies and buildings.

5.2. Mis-Extraction of Shadow Interference

Figures 10 and 13 demonstrate that despite the SMBWI performing the best among all tested water indices in eliminating shadow interference, there are also a few flaws in the extraction results. This is due to the similar spectral characteristics of shadows and water, particularly in the visible light bands, which makes it difficult for water indices to accurately distinguish between water bodies and shadows [9,44–46].

Among various types of shadows, cloud shadows are the most common, and the problem can occur in high- and medium-spatial-resolution imagery [46]. Additionally, the reflectance spectral characteristics of cloud shadows vary with different underlying surface materials [44,47]. In Figure 10, cloud shadows mainly cover vegetation, leading to lower reflectance in these areas compared to unshaded vegetation areas. This is evident in Figure 3, where the reflectance curve of cloud shadows is similar to vegetation because the area covered by the cloud shadow is vegetation, but the reflectance is generally lower than that of unshaded vegetation.

By considering more near-infrared bands (B8, B8A and B9) in the formula when constructing water indices, the distinct spectral differences between water bodies and non-water bodies in the near-infrared bands are used, which may be more effective to distinguish water bodies from shadows. Therefore, we considered multiple near-infrared bands in the SMBWI calculating equation, which has been proven to distinguish water bodies more effectively from shadows.

5.3. Mixed Pixels' Misidentification

When addressing mixed water and non-water pixels, the SMBWI generally shows the lowest errors, but tends to omit a significant proportion of mixed pixels with water contents between 50% and 70%. Analysis of Figure 16 reveals that all indices typically produce higher total errors in mixed pixels with medium water contents (30% to 70%).

This phenomenon stems from the fact that within the range of water contents, water and non-water are almost equally mixed, causing the indicator value to hover near the threshold. These indicator values are not significantly close to either water or non-water, resulting in higher omission errors. Moreover, as can be observed in Tables 4–8 and A2, the omission error (OE) values for the SMBWI are not the best among the nine water indices examined, which may be related to the SMBWI's higher OE in mixed pixels with water contents between 50% and 70%. The ability of water indices to accurately distinguish mixed pixels with medium water contents could potentially indicate their effectiveness in identifying mixed pixels.

5.4. Limitation of the SMBWI

Despite the SMBWI's impressive performance in our tests, it still has its limitations and/or potential for improvement. The SMBWI uses the unique B8A band of Sentinel-2, which helps to distinguish water bodies from land cover more effectively [22]. However, the B8A band is typically absent for other optical remote sensing satellites, which limits the application of the SMBWI with all kinds of optical satellite data. In the future, for optical satellite data that do not include B8A, we need to find other alternative near-infrared bands.

6. Conclusions

In this paper, a new and robust water index called the Sentinel Multi-Band Water Index (SMBWI) was proposed to extract water bodies in complex environments with Sentinel-2 satellite imagery.

To investigate the effectiveness of the SMBWI in eliminating the interference of complex environments, six test sites with special interfering land cover features were selected, and water bodies were extracted with the SMBWI and eight commonly used water indices. The SMBWI showed the best performance in eliminating interference from urban built-up areas (and their shadows), cultivated lands, vegetation and clouds (and cloud shadows), alpine terrain with bare ground and glaciers. Additionally, the SMBWI also performed very well in detecting small water bodies and identifying mixed pixels. Both qualitative and quantitative comparisons indicated that the SMBWI is better than the other eight traditional water indices in extracting water bodies under complex interfering environments of land cover features from Sentinel-2 satellite imagery.

The new and effective water index, the SMBWI, provides a means of extracting land surface water bodies with Sentinel-2 imagery, which is useful for surveying land surface water bodies and delineating their spatial distribution.

Author Contributions: Conceptualization, L.X. and Z.S.; methodology, L.X. and Z.S.; software, Z.S. and L.X.; validation, L.X., Z.S., H.S., L.J., F.D., W.W., K.H., J.G., A.N., H.C. and P.G.; formal analysis, L.X., Z.S. and H.S.; investigation, L.X., Z.S., L.J., F.D., W.W., K.H., J.G., A.N., H.C. and P.G.; resources, L.X., Z.S. and H.S.; data curation, L.X. and Z.S.; writing—original draft preparation, Z.S. and L.X.; writing—review and editing, L.X., Z.S., H.S., L.J., F.D., W.W., K.H., J.G., A.N., H.C. and P.G.; visualization, L.X. and Z.S.; supervision, L.X. and H.S.; project administration, L.X.; funding acquisition, L.X., L.J., F.D. and H.C. All authors have read and agreed to the published version of the manuscript.

Funding: This research was funded by the National Natural Science Foundation of China (42004007, 42274117); the Open Fund of the National Engineering Research Center of Geographic Information System (2023KFJJ12); the Hubei Key Research and Development Program (2023DJC154); and the Science and Technology Research Project of Hubei Provincial Department of Education (Q20221306).

Data Availability Statement: The data supporting the conclusions of this article will be made available by the authors on request.

Acknowledgments: We are grateful to the European Space Agency (ESA) for providing the optical remote sensing images from Sentinel-2 used in this study.

Conflicts of Interest: The authors declare no conflicts of interest.

Appendix A

Appendix A.1. Supplementary Experiment on Extracting Small Water Bodies

To investigate the SMBWI's ability to extract small water bodies, we select the area on the east of the Dagang Reservoir where many small artificial reservoirs are scattered. Considering the small size of these water bodies, we combined high-resolution Google satellite imagery with manual visual interpretation to identify their distribution, which served as the benchmark for real small water body areas. Subsequently, the area of the small water bodies extracted using the water index was compared with the real area to calculate the extraction error of water body area (EA), using the equation:

$$EA = \frac{|t_0 - t_i|}{t_0} \times 100, \tag{A1}$$

where t_0 is the real small water body area obtained by visual interpretation, and t_i is the small water body area obtained by the water indices. We selected satellite imagery of 23 October 2020, close to the imaging time of Google Maps. The visual interpretation results are shown in Figure A1a, while extraction results by the SMBWI, MNDWI and RNDWI are

shown in Figure A1b–d, respectively, displaying the results from the water indices with the lowest or highest EAs in extracting small water bodies. The actual total area of the small water bodies obtained through visual interpretation in the region is 0.3763 km². Combining with areas derived from water indices, the EA results of nine water indices are presented in Table A1, among which the SMBWI shows the lowest area error of 2.07%. Thus, the SMBWI performs the best in extracting small water bodies among the water indices, while the MNDWI and RNDWI have higher EAs due to mis-extraction of buildings and roads as water bodies.

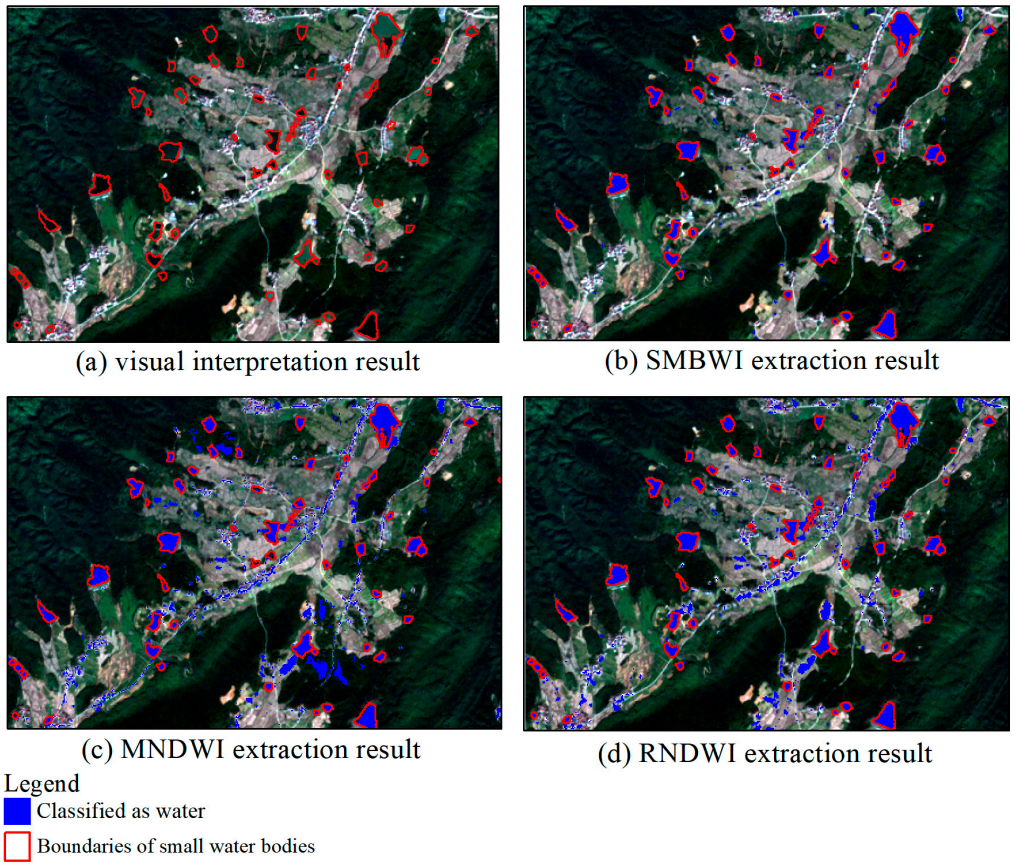


Figure A1. Visual interpretation results and water body extraction results for small water bodies on the east of Dagang Reservoir. (**a**) The selected verification area, with red lines enclosing the small water bodies through visual interpretation. (**b**–**d**) the water bodies extracted by SMBWI, MNDWI and RNDWI, respectively, with water bodies in blue, overlying the original imagery.

Table A1. Extraction error of water body area (EA) from nine tested indices for small water bodies.

	SMBWI	**MBWI**	**AWEI$_{nsh}$**	**SWI**	**NDWI**	**AWEI$_{sh}$**	**RWI**	**MNDWI**	**RNDWI**
Area (km^2)	0.3841	0.3323	0.3288	0.4350	0.4504	0.4552	0.5831	0.6355	0.7172
EA (%)	2.07%	11.69%	12.62%	15.60%	19.69%	20.97%	54.96%	68.88%	90.59%

Appendix A.2. Supplementary Experiment of Alpine Terrain and Glacier Interference Elimination

In the study of the Hala Lake Basin, test site 4, the SMBWI demonstrated an excellent water body extraction performance in eliminating glacier interference compared to other water indices. For further confirmation, we selected the Taiyang Lake Basin, which has similar land cover features to the Hala Lake Basin. As shown in Figure A2b–j, the extraction result of the SMBWI is still the best without white patches in glacier-covered areas, while other water indices exhibit varying quantities of white patches there. In Figure A3, at the

boundary of a glacier, we show the detailed extraction results of the three water indices that performed the best and the worst. Here, the SMBWI does not show mis-extraction, while the RNDWI and SWI display extensive blue patches caused by glaciers, clouds and their shadows.

An accuracy evaluation using 100 water and 250 non-water validation sample points, summarized in Table A2, highlights the best performance of the SMBWI, with a Kappa value of 0.96, an overall accuracy (OA) of 98.26% and a total error (TE) of 6.04%.

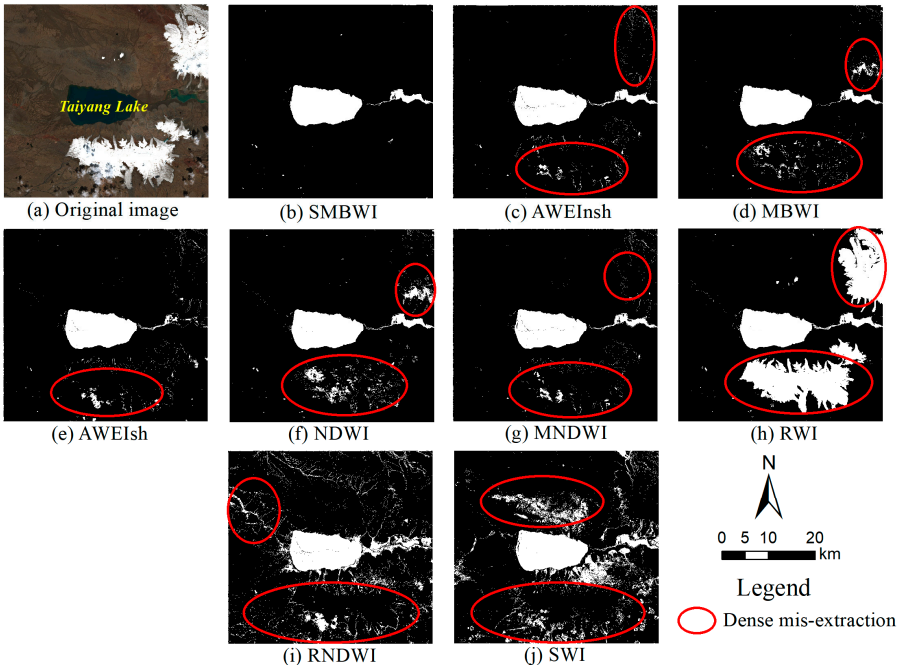


Figure A2. As Figure 14, but for the supplementary experiment at test site 5, Taiyang Lake Basin.

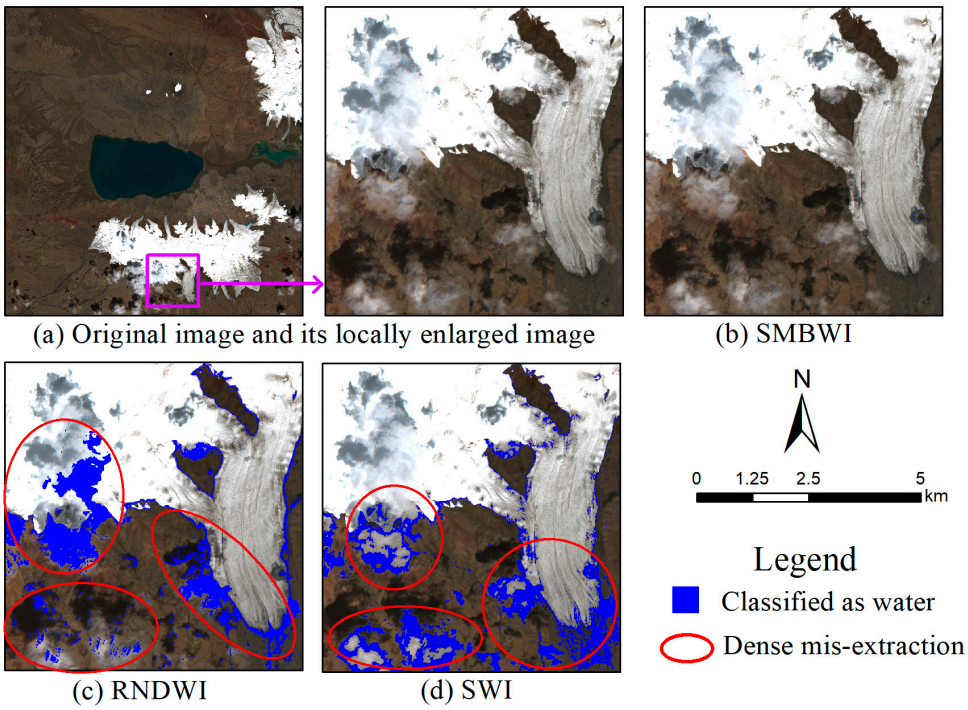


Figure A3. As Figure 15, but for the supplementary experiment at test site 5, Taiyang Lake Basin.

Table A2. As Table 7, but for the supplementary experiment at test site 5, Taiyang Lake Basin.

Test Site	Water Index	OA (%)	Kappa	PA (%)	UA (%)	OE (%)	CE (%)	TE (%)
5 (Taiyang Lake)	SMBWI	98.26	0.96	96.00	97.96	4.00	2.04	6.04
	$AWEI_{nsh}$	93.71	0.85	89.00	89.00	11.00	11.00	22.00
	MBWI	89.71	0.76	87.00	79.09	13.00	20.91	33.91
	$AWEI_{sh}$	90.29	0.75	77.00	87.50	23.00	12.50	35.50
	NDWI	88.86	0.74	89.00	76.07	11.00	23.93	34.93
	MNDWI	89.71	0.73	70.00	92.11	30.00	7.89	37.89
	RWI	84.86	0.65	86.00	68.80	14.00	31.20	45.20
	RNDWI	82.57	0.59	75.00	67.57	25.00	32.43	57.43
	SWI	80.29	0.54	75.00	63.03	25.00	36.97	61.97

References

1. Du, Y.; Zhang, Y.; Ling, F.; Wang, Q.; Li, W.; Li, X. Water bodies' mapping from Sentinel-2 imagery with modified normalized difference water index at 10-m spatial resolution produced by sharpening the SWIR band. *Remote Sens.* **2016**, *8*, 354. [CrossRef]
2. Jiang, W.; Ni, Y.; Pang, Z.; Li, X.; Ju, H.; He, G.; Lv, J.; Yang, K.; Fu, J.; Qin, X. An effective water body extraction method with new water index for sentinel-2 imagery. *Water* **2021**, *13*, 1647. [CrossRef]
3. Yang, Y.; Liu, Y.; Zhou, M.; Zhang, S.; Zhan, W.; Sun, C.; Duan, Y. Landsat 8 OLI image based terrestrial water extraction from heterogeneous backgrounds using a reflectance homogenization approach. *Remote Sens. Environ.* **2015**, *171*, 14–32. [CrossRef]
4. Papa, F.; Prigent, C.; Rossow, W.B. Monitoring flood and discharge variations in the large Siberian rivers from a multi-satellite technique. *Surv. Geophys.* **2008**, *29*, 297–317. [CrossRef]
5. Vörösmarty, C.J.; Sharma, K.P.; Fekete, B.M.; Copeland, A.H.; Holden, J.; Marble, J.; Lough, J.A. The storage and aging of continental runoff in large reservoir systems of the world. *Ambio* **1997**, *26*, 210–219.
6. Pan, F.; Xi, X.; Wang, C. A comparative study of water indices and image classification algorithms for mapping inland surface water bodies using Landsat imagery. *Remote Sens.* **2020**, *12*, 1611. [CrossRef]
7. Huang, C.; Chen, Y.; Zhang, S.; Wu, J. Detecting, extracting, and monitoring surface water from space using optical sensors: A review. *Rev. Geophys.* **2018**, *56*, 333–360. [CrossRef]
8. Wang, C.; Zhang, J.; Li, Y. Phoumilay. The construction and verification of a water index in the complex environment based on GF-2 images. *Remote Sens. Nat. Resour.* **2022**, *34*, 50–58.
9. Feyisa, G.L.; Henrik, M.; Rasmus, F.; Simon, R.P. Automated Water Extraction Index: A new technique for surface water mapping using Landsat imagery. *Remote Sens. Environ.* **2014**, *140*, 23–35. [CrossRef]
10. Zhang, C.; Lv, A.; Zhu, W.; Yao, G.; Qi, S. Using multisource satellite data to investigate lake area, water level, and water storage changes of terminal lakes in ungauged regions. *Remote Sens.* **2021**, *13*, 3221. [CrossRef]
11. Onačillová, K.; Gallay, M.; Paluba, D.; Péliová, A.; Tokarčík, O.; Laubertová, D. Combining Landsat 8 and Sentinel-2 Data in Google Earth Engine to Derive Higher Resolution Land Surface Temperature Maps in Urban Environment. *Remote Sens.* **2022**, *14*, 4076. [CrossRef]
12. Fisher, A.; Danaher, T. A water index for SPOT5 HRG satellite imagery, New South Wales, Australia, determined by linear discriminant analysis. *Remote Sens.* **2013**, *5*, 5907–5925. [CrossRef]
13. Xie, C.; Huang, X.; Zeng, W.; Fang, X. A novel water index for urban high-resolution eight-band WorldView-2 imagery. *Int. J. Digit. Earth* **2016**, *9*, 925–941. [CrossRef]
14. Sharma, R.C.; Tateishi, R.; Hara, K.; Luong, V.N. Developing superfine water index (SWI) for global water cover mapping using MODIS data. *Remote Sens.* **2015**, *7*, 13807–13841. [CrossRef]
15. Ji, L.; Zhang, L.; Wylie, B. Analysis of dynamic thresholds for the normalized difference water index. *Photogramm. Eng. Remote Sens.* **2009**, *75*, 1307–1317. [CrossRef]
16. Proud, S.R.; Fensholt, R.; Rasmussen, L.V.; Sandholt, I. Rapid response flood detection using the MSG geostationary satellite. *Int. J. Appl. Earth Obs. Geoinf.* **2011**, *13*, 536–544. [CrossRef]
17. Rad, A.M.; Kreitler, J.; Sadegh, M. Augmented Normalized Difference Water Index for improved surface water monitoring. *Environ. Model. Softw.* **2021**, *140*, 105030. [CrossRef]
18. Rees, W.G. *Physical Principles of Remote Sensing*, 3rd ed.; Cambridge University Press: New York, NY, USA, 2013.
19. Hollstein, A.; Segl, K.; Guanter, L.; Brell, M.; Enesco, M. Ready-to-use methods for the detection of clouds, cirrus, snow, shadow, water and clear sky pixels in Sentinel-2 MSI images. *Remote Sens.* **2016**, *8*, 666. [CrossRef]
20. McFeeters, S.K. The use of the Normalized Difference Water Index (NDWI) in the delineation of open water features. *Int. J. Remote Sens.* **1996**, *17*, 1425–1432. [CrossRef]
21. Xu, H. Modification of normalised difference water index (NDWI) to enhance open water features in remotely sensed imagery. *Int. J. Remote Sens.* **2006**, *27*, 3025–3033. [CrossRef]

22. Wu, Q.S.; Wang, M.X.; Shen, Q.; Yao, Y.; Li, J.S.; Zhang, F.F.; Zhou, Y.M. Small water body extraction method based on Sentinel-2 satellite multi-spectral remote sensing image. *Natl. Remote Sens. Bull.* **2022**, *26*, 781–794. [CrossRef]
23. Cao, R.; Li, C.; Liu, L.; Wang, J.; Yan, G. Extracting Miyun reservoir's water area and monitoring its change based on a revised normalized different water index. *Sci. Surv. Mapp.* **2008**, *33*, 158–160.
24. Wang, X.; Xie, S.; Zhang, X.; Chen, C.; Guo, H.; Du, J.; Duan, Z. A robust Multi-Band Water Index (MBWI) for automated extraction of surface water from Landsat 8 OLI imagery. *Int. J. Appl. Earth Obs. Geoinf.* **2018**, *68*, 73–91. [CrossRef]
25. Chen, W.; Ding, J.; Li, Y.; Niu, Z. Extraction of water information based on China-made GF-1 remote sense image. *Resour. Sci.* **2015**, *37*, 1166–1172.
26. Li, D.; Wu, B.S.; Chen, B.W.; Xue, Y.; Zhang, Y. Review of water body information extraction based on satellite remote sensing. *J. Tsinghua Univ. (Sci. Technol.)* **2020**, *60*, 147–161.
27. Yang, X.C.; Qin, Q.M.; Grussenmeyer, P.; Koehl, M. Urban surface water body detection with suppressed built-up noise based on water indices from Sentinel-2MSI imagery. *Remote Sens. Environ.* **2018**, *219*, 259–270. [CrossRef]
28. Wang, X.; Gong, Z.; Pu, R. Estimation of chlorophyll a content in inland turbidity waters using WorldView-2 imagery: A case study of the Guanting Reservoir, Beijing, China. *Environ. Monit. Assess.* **2018**, *190*, 620. [CrossRef] [PubMed]
29. Torbick, N.; Hu, F.; Zhang, J.; Qi, J.; Zhang, H.; Becker, B. Mapping chlorophyll-a concentrations in West Lake, China using Landsat 7 ETM+. *J. Great Lakes Res.* **2008**, *34*, 559–565. [CrossRef]
30. Yao, F.; Wang, C.; Dong, D.; Luo, J.; Shen, Z.; Yang, K. High-resolution mapping of urban surface water using ZY-3 multi-spectral imagery. *Remote Sens.* **2015**, *7*, 12336–12355. [CrossRef]
31. Drusch, M.; Del Bello, U.; Carlier, S.; Colin, O.; Fernandez, V.; Gascon, F.; Hoersch, B.; Isola, C.; Laberinti, P.; Martimort, P.; et al. Sentinel-2: ESA's Optical High-Resolution Mission for GMES Operational Services. *Remote Sens. Environ.* **2012**, *120*, 25–36. [CrossRef]
32. Yang, X.C.; Chen, Y.; Wang, J.Z. Combined use of Sentinel-2 and Landsat 8 to monitor water surface area dynamics using Google Earth Engine. *Remote Sens. Lett.* **2020**, *11*, 687–696. [CrossRef]
33. Peltoniemi, J.I.; Suomalainen, J.; Puttonen, E.; Näränen, J.; Rautiainen, M. Reflectance properties of selected arctic-boreal land cover types: Field measurements and their application in remote sensing. *Biogeosci. Discuss.* **2008**, *5*, 1069–1095.
34. Abbas, A.W.; Minallh, N.; Ahmad, N.; Abid, S.A.R.; Khan, M.A.A. K-Means and ISODATA clustering algorithms for landcover classification using remote sensing. *Sindh Univ. Res. J.-SURJ (Sci. Ser.)* **2016**, *48*, 315–318.
35. Li, X.; Liu, L.; Huang, L. Comparison of several remote sensing image classification methods based on envi. *Int. Arch. Photogramm. Remote Sens. Spat. Inf. Sci.* **2020**, *42*, 605–611. [CrossRef]
36. Ji, H.X.; Fan, X.W.; Wu, G.P.; Liu, Y.B. Accuracy comparison and analysis of methods for water area extraction of discrete lakes. *J. Lake Sci.* **2015**, *27*, 327–334.
37. Liu, S.; Wu, Y.; Zhang, G.; Lin, N.; Liu, Z. Comparing Water Indices for Landsat Data for Automated Surface Water Body Extraction under Complex Ground Background: A Case Study in Jilin Province. *Remote Sens.* **2023**, *15*, 1678. [CrossRef]
38. Tian, Q.; Zhao, H.J.; Lin, Y.; Xiao, F.J. Performance Evaluation of Machine Learning in Wireless Connected Robotics Swarms. *IEEE Access* **2019**, *8*, 1790–1802. [CrossRef]
39. Fitzgerald, R.W.; Lees, B.G. Assessing the classification accuracy of multisource remote sensing data. *Remote Sens. Environ.* **1994**, *47*, 362–368. [CrossRef]
40. Barsi, Á.; Kugler, Z.; László, I.; Szabó, G.; Abdulmutalib, H.M. Accuracy dimensions in remote sensing. *Int. Arch. Photogramm. Remote Sens. Spat. Inf. Sci.* **2018**, *42*, 61–67. [CrossRef]
41. Wang, X.; Xie, S.; Du, J. Water index formulation and its effectiveness research on the complicated surface water surroundings. *J. Remote Sens.* **2018**, *22*, 360–372. [CrossRef]
42. Moreira, R.D.C.; Galvão, L.S. Variation in spectral shape of urban materials. *Remote Sens. Lett.* **2010**, *1*, 149–158. [CrossRef]
43. Ye, C.M.; Cui, P.; Pirasteh, S.; Li, J.; Li, Y. Experimental approach for identifying building surface materials based on hyperspectral remote sensing imagery. *J. Zhejiang Univ.-SCIENCE A* **2017**, *18*, 984–990. [CrossRef]
44. Zhai, H.; Zhang, H.; Zhang, L.; Li, P. Cloud/shadow detection based on spectral indices for multi/hyperspectral optical remote sensing imagery. *ISPRS J. Photogramm. Remote Sens.* **2018**, *144*, 235–253. [CrossRef]
45. AlMaazmi, A. Water bodies extraction from high resolution satellite images using water indices and optimal threshold. *Image Signal Process. Remote Sens. XXII* **2016**, *10004*, 509–521.
46. Shahtahmassebi, A.; Yang, N.; Wang, K.; Moore, N.; Shen, Z. Review of shadow detection and de-shadowing methods in remote sensing. *Chin. Geogr. Sci.* **2013**, *23*, 403–420. [CrossRef]
47. Liu, W.; Yamazaki, F. Object-based shadow extraction and correction of high-resolution optical satellite images. *IEEE J. Sel. Top. Appl. Earth Obs. Remote Sens.* **2012**, *5*, 1296–1302. [CrossRef]

Disclaimer/Publisher's Note: The statements, opinions and data contained in all publications are solely those of the individual author(s) and contributor(s) and not of MDPI and/or the editor(s). MDPI and/or the editor(s) disclaim responsibility for any injury to people or property resulting from any ideas, methods, instructions or products referred to in the content.